High-density amorphous ice: Molecular dynamics simulations of the glass transition at 0.3 GPa

M. Seidl,[1,2] T. Loerting,[1] and G. Zifferer[2,a]

[1]*Institute of Physical Chemistry, University of Innsbruck, Innrain 52a, A-6020 Innsbruck, Austria*
[2]*Department of Physical Chemistry, University of Vienna, Währinger Str. 42, A-1090 Wien, Austria*

Based on several force fields (COMPASS, modified TIP3P and SPC/E) high-density amorphous ice is simulated by use of isothermal-isobaric molecular dynamics at a pressure of $p \approx 0.3$ GPa in the temperature range from 70 to 300 K. Starting at low temperature a large number of heating/cooling cycles are performed and several characteristic properties (density, total energy, and mobility) are traced as functions of temperature. While the first cycles are showing irreversible structural relaxation effects data points from further cycles are reproducible and give clear evidence for the existence of a glass-to-liquid transition. Although, the observed transition temperatures T_g are dependent on the actual force field used and slightly dependent on the method adopted the results indicate that high-density amorphous ices may indeed be low-temperature structural proxies of ultraviscous high-density liquids. © *2009 American Institute of Physics.* [doi:10.1063/1.3224857]

I. INTRODUCTION

Despite the rather simple structure of the molecule, water exhibits several anomalies and the phase diagram is rather complex and yet incomplete. Apart from at least 15 (crystalline) ice phases[1] supercooled water exists in (noncrystalline) amorphous, i.e., glassy state which in addition is showing polyamorphism: at least five methods have been used to produce amorphous ice[2,3] which can be categorized into three distinct structural states, namely, low-density amorphous (LDA), high-density amorphous (HDA), and very high-density amorphous (VHDA) ice.[4,5]

LDA ice exhibits a so-called glass-to-liquid transition[6] to a low-density liquid (LDL), i.e., relaxation dynamics changes at a certain temperature ($T_g \approx 136$ K at 1 bar)[7] from the one typical for a glassy solid to the one typical for a (deeply) supercooled liquid.[8] On continued heating LDL crystallizes at $T_X \approx 150$ K (1 bar).[7] By contrast to melting the glass-to-liquid transition is not a phase transition in the strict thermodynamic sense, but is affected by the thermal history of the glass and on varying heating/cooling rates.

It is still unresolved whether there are also deeply supercooled liquids emanating on heating HDA (and also VHDA). On the one hand high-pressure dielectric relaxation studies[9] and high-pressure vitrification studies[10] as well as our own high-pressure dilatometry studies[11] suggest the existence of the deeply supercooled high-density liquid (HDL). On the other hand quasiharmonic lattice dynamics calculations suggest that at $T < 162$ K HDA is produced from hexagonal ice by a mechanical collapse of water molecules into empty interstitial sites rather than by thermodynamic melting at $p > 1$ GPa, which calls into question the validity of there being a thermodynamic connection between the amorphous and liquid phases of water.[12] This process of pressure induced melting and amorphization of hexagonal ice was shown by piston-cylinder experiments to change from two-phase equilibrium melting at $T > 165$ K to a one-phase amorphization to an unrelaxed phase at $T < 165$ K related to HDA,[13] which was also corroborated from neutron scattering data revealing the role of phonon softening.[14] Furthermore, neutron scattering and diffraction studies reveal a heterogeneous character in HDA, while VHDA and LDA appear as homogeneous structures.[15] In this sense HDA could be viewed as nanocrystalline material unrelated to a deeply supercooled liquid. This apparent contradiction in the literature was addressed also by computer simulations, unfortunately again with contradicting results. While some simulations interpret VHDA to be the quenched amorphous ice of HDL (Ref. 16) or infer a region of highly compressible HDL so that a whole branch of HDA states is a good candidate to be the quenched amorphous ices of HDLs,[17] others acknowledge the possibility of up to four amorphous ices thermodynamically connected to up to four supercooled liquids.[18]

Computer simulation methods offer highly efficient routes for the investigation of properties of amorphous species.[19] Many force fields have been employed for simulations of supercooled water and amorphous ices over the past two decades.[17,18,20] By contrast to experiments, at the ultrahigh heating rates employed in molecular dynamics simulations crystallization does not occur and therefore interfere in the vicinity of T_g. Thus, if a glass-to-liquid transition from HDA to HDL exists it should be directly reflected in the simulation, although one cannot expect to obtain a quantitative prediction of the value of T_g as the transition temperatures depend on the force field as well as on the heating/cooling rate as stated above. Therefore, in the present investigation isothermal-isobaric molecular dynamics simulations based on several force fields, i.e., COMPASS and modified versions of the transferable intermolecular potential TIP3P and the extended simple point charge model SPC/E,

a)Author to whom correspondence should be addressed. Electronic mail: gerhard.zifferer@univie.ac.at.

respectively, are performed on the glass-to-liquid transition. Starting with an amorphous model system of water at a density corresponding to HDA at low temperatures several heating and cooling runs are simulated at a pressure of 0.3 GPa in order to directly simulate relaxation followed by dilatometry experiments, i.e., the determination of T_g from a kink in the density versus temperature curve[21] as soon as reproducibility on heating/cooling is attained. In addition, corroborating information is obtained from enthalpy versus T curves and the T-dependence of molecular mobility. While some simulation work has been devoted to studying the glass-to-liquid transition in LDA,[22] we are not aware of any literature study analyzing the possibility of a glass-to-liquid transition in HDA or VHDA apart from our preliminary investigation on this subject.[23]

II. COMPUTATIONAL METHOD

The *NPT* (constant pressure and temperature) molecular dynamics simulations were performed by use of Materials Studio® 4.4 from Accelrys, Inc. with module *Amorphous Cell* for the preparation of the systems and module *Discover* as molecular dynamics engine using the Andersen thermostat[24] and barostat[25] with a time step of 1 fs applying the Verlet velocity algorithm.[26] A cutoff distance of 1.25 nm with a spline switching function (0.3 nm width) was applied for the nonbonding interactions making use of charge groups in order to prevent dipoles from being artificially split when one of the atoms was inside and another was outside the atom-based cutoff. Three different force fields have been used in this investigation:

The (commercial) force field COMPASS (condensed-phase optimized molecular potentials for atomistic simulation studies) from Accelrys, Inc. is a class-II force field optimized for the simulation of condensed phases, see Refs. 27 for parametrization and validation. The water model incorporated in COMPASS is a simple three-point model with atom charges $q_O=-0.82e$ and $q_H=+0.41e$, the unperturbed bond length and bond angle reading as $l_0=0.0957$ nm and $\theta_0=104.52°$, respectively. Bond length l and angle θ are not rigid in COMPASS but modeled as sums of harmonic terms $k_{l,n}(l-l_0)^n$ and $k_{\theta,n}(\theta-\theta_0)^n$, respectively, with $n=2, 3, 4$, further including bond-bond and bond-angle cross terms. Force field parameters were parametrized for simulations close to ambient temperature-conditions and below.[28]

More common potentials for water simulations are the TIP3P (Ref. 29) and SPC/E (Ref. 30) force fields with rigid bonds and angles ($l_0=0.095\ 72$ nm, $\theta_0=104.52°$ for TIP3P and $l_0=0.1$ nm, $\theta_0=109.47°$ for SPC/E). In the present investigation flexible molecules TIP3P* and SPC/E* are defined with harmonic bond and angle potentials (quadratic terms only and no cross terms) using the bond and angle parameters of TIP3P and SPC/E, respectively, for the unperturbed values and the potential function parameters of the CVFF force field,[31] i.e., $k_l=22.62$ kJ nm^{-2} and $k_\theta=209.2$ kJ deg^{-2} and taking the nonbond parameters (van der Waals and Coulomb terms) from the original TIP3P and SPC/E force fields.
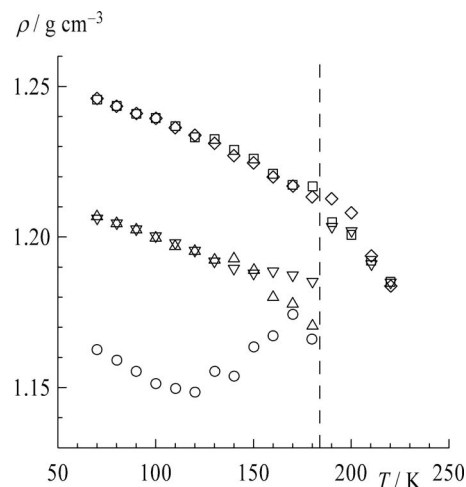

FIG. 1. Density vs temperature profiles for first heating (circles) and cooling (triangles), second heating (inverted triangles) and cooling (squares), and for a third heating run (diamonds) using the COMPASS force field. The broken vertical line indicates T_g obtained from Fig. 3(a).

III. RESULTS AND DISCUSSION

A. Preparation of the initial system

The experimentally[3] determined density of HDA at 70 K and 1 bar is 1.16 g/cm^3, while it is expected and even known from a previous preliminary simulation[23] that the density of HDA at the chosen simulation pressure of 0.3 GPa is larger (≈ 1.23 g/cm^3). Nevertheless, the initial system has been prepared at the 1 bar density to avoid to prejudge the results and to allow the system to find its characteristic density upon relaxation.

Thus, by use of the Amorphous Cell tool a cubic box (with periodic boundaries in all directions) with a box length of ≈ 2.98 nm was filled with $N=1024$ water molecules (force field COMPASS) followed by a small energy minimization run to remove energetically unfavorable configurations. Then the system was relaxed by several heating/cooling cycles as described in detail in Sec. III B. In Fig. 1 the density versus temperature profiles are shown. Starting at 70 K the system was heated to 180 K (circles), cooled to 70 K (triangles), heated to 220 K (inverted triangles), and cooled to 70 K (squares). During this process the density at 70 K increased to ≈ 1.25 g/cm^3. The following heating run (diamonds) and further heating/cooling cycles closely follow the course of the second cooling run, see Sec. III B.

For the TIP3P* and SPC/E* simulations a relaxed configuration obtained by use of COMPASS was used for initialization followed by two heating/cooling cycles in the range from 70 to 90 K to allow the system to rearrange due to the new parameters.

Although the parameters of the SPC/E* system are quite different compared to COMPASS the 70 K density stayed almost the same. In Fig. 2 the density versus temperature profiles are shown. Heating to 220 K (circles) and cooling to 70 K (triangles) changed the 70 K density to ≈ 1.20 g/cm^3 and further cycles (black dots) exhibited a nearly linear relationship between density and temperature. However, upon heating to 250 K (inverted triangles) the density increased between 220 and 240 K and after cooling to 70 K (squares)
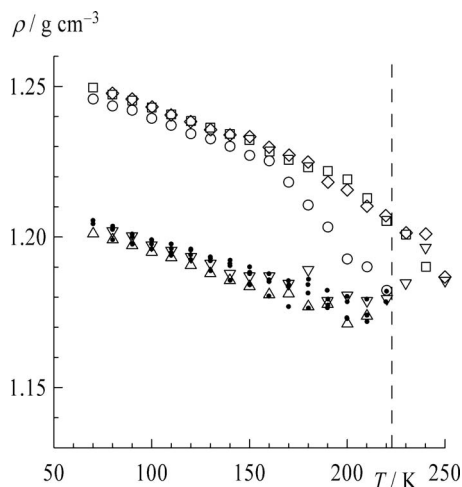
FIG. 2. Density vs temperature profiles for first heating (circles) and cooling (triangles), several cycles between 70 and 220 K (black dots) followed by heating up to 250 K (inverted triangles), and a further cooling/heating cycle (squares/diamonds) using the SPC/E* force field. The broken vertical line indicates T_g obtained from Fig. 3(c).

the initial density of ≈ 1.25 g/cm^3 was restored. The next heating run (diamonds) and all further cycles between 70 and 260 K exhibited comparable results, see Sec. III B.

The density of the TIP3P* system at 70 K immediately increased to ≈ 1.28 g/cm^3 and remained unchanged during further cycles over the full range of temperatures (70–250 K). Thus, a diagram of the initial relaxation runs is omitted.

B. Density profiles

In order to allow for relaxation (see Sec. III A) and to simulate the density ρ versus temperature T curve (which in turn yields the basis for the determination of T_g), the system was heated in steps of 10 K until a maximum temperature was reached. Afterward, a cooling process was initiated by lowering the temperature in steps of 10 K until the lowest temperature (70 K) was reached. Then, the cycle was started again. At each temperature a 500 ps run was performed (250 ps for equilibration and 250 ps for data sampling) using the final configuration of a run as the starting structure for the next temperature (10 K higher or lower). A similar temperature program has been already successfully used in previous simulations on the glass transition of polymers[32] and carbohydrates.[33]

It should be noted that the instantaneous pressure p_i (calculated by use of the virial theorem) fluctuates by $\approx 100\%$, i.e., the range of pressures amounts from ≈ 0 (actually slightly negative values) to ≈ 0.6 GPa, the average value slightly decreasing with T. However, restriction to systems with $0.27 < p_i/\mathrm{GPa} < 0.33$, thus allowing for 10% deviation from the target value only, results in average values, which are identical to those of the whole ensemble within graphical resolution.

In Fig. 3 these dilatometric simulation curves are shown. Results of several cycles ($5 \times$ heating and $5 \times$ cooling for COMPASS and TIP3P*, four full cycles for SPC/E*) are depicted as black dots, the maximum temperature reading as 220 K for COMPASS, 250 K for TIP3P*, and 260 K for
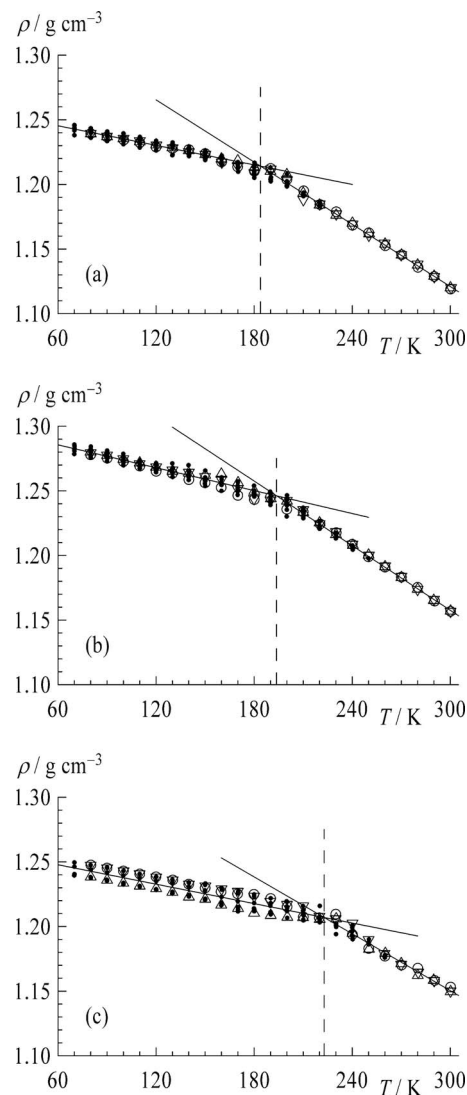

FIG. 3. Density vs temperature profiles for the (a) COMPASS, (b) TIP3P*, and (c) SPC/E* force fields. Dots refer to [(a) and (b)] five or (c) four heating/cooling cycles in the range from 70 to (a) 220 K to (b) 250 K and to (c) 260 K followed by three independent heating runs up to 300 K (symbols). Straight lines are obtained by linear regression of data points belonging to $T < 160$ K and $T > 220$ K, respectively. The intersections reading as (a) 183.9 K, (b) 193.7 K, and (c) 222.8 K represent T_g, indicated by vertical broken lines.

SPC/E*. The last heating run (indicated by circles) was extended to 300 K. In addition, two further independent heating runs up to 300 K are shown as well (triangles). Close inspection of Fig. 3(a) (COMPASS force field) and analyzing the standard deviation (std) of the data points reveals three regions. Up to $T = 170$ K std/(g cm^{-3}) amounts ≈ 0.0075, between 180 and 200 K 0.010–0.012, at 210 K ≈ 0.005 and then steadily decreases to ≈ 0.0005 at 300 K. Above and below the intermediate region with rather large fluctuations are two sections with linear dependence of density on temperature, the slope at low temperature being smaller than the slope at high temperatures. The two lines result from fitting a straight line to data points corresponding to $T < 160$ K and $T > 220$ K, respectively, and intersect at $T \approx 184$ K, which may be interpreted as a glass transition temperature $T_g \approx 184$ K for the transition from glassy HDA (at low tem-

peratures) to an ultraviscous liquid HDL (at higher temperatures). As fluctuations are largest close to T_g, the fluctuating behavior in the middle region corroborates the existence of a glass transition and results in an estimate of its width of about 30 K at the heating/cooling rates employed in the simulation. For TIP3P* [Fig. 3(b)] the situation is quite similar with $T_g \approx 194$ K. For SPC/E* the range of ρ values at a given temperature is appreciably broader in the glassy region than for the other models and the extracted transition is at still larger temperatures $T_g \approx 223$ K. Intersection of a line through data points at the lower (upper) boundary in the amorphous region with the regression line in the high temperature region appears at $T \approx 231$ K ($T \approx 208$ K) again suggesting a glass transition width of about 20–30 K. The upper limit 160 K and lower limit 220 K chosen above are somewhat arbitrary, of course; shifting the limits to 130 and 250 K, respectively, yields estimates for T_g reading as 188 K (COMPASS), 197 K (TIP3P*), and 216 K (SPC/E*).

To summarize, although there is no quantitative correspondence all water models provided exhibit a clear-cut glass transition.

C. Energy and enthalpy

In Fig. 4 the potential energy U and the total energy (enthalpy) H (both in kilojoule per mole water, where the latter is calculated from the simulations as the sum of potential energy, kinetic energy, and pV) are plotted as a function of temperature. For all three models at a certain temperature the data points clearly deviate from linearity, which is again indicative of the glass-to-liquid transition. As a guide to the eye two curves, a straight line obtained by linear regression of data points below $T = 160$ K and a polynomial regression of data points larger than $T = 220$ K, are shown, which fit to the glassy state data points at temperatures below the intersection point and to the liquid state data points at temperatures above. The kink in the $H(T)$ curve appears at the same temperature as the kink in $U(T)$ and the corresponding temperatures read as ≈ 178 K for COMPASS, ≈ 190 K for TIP3P*, and ≈ 214 K for SPC/E* in accordance with the glass transition temperatures obtained from the density profiles, see Sec. III B. A method for the determination of T_g is based on the stepwise increase in the molar heat capacity $c_p(T)$ typically obtained in differential scanning calorimetry (DSC) experiments.[6] As c_p is the first derivative of $H(T)$ with respect to T the kink in $H(T)$ is directly connected with the change in $c_p(T)$ at T_g.

D. Molecular mobility

In addition to the $\rho(T)$ and $H(T)$ versus T plots, T_g may also be derived from a change in the molecular mobility, e.g., characterized by the diffusion coefficient D. D can be extracted from a plot of the mean square displacement (msd_t) of oxygen atoms versus time,[34,35]

$$msd_t = \langle |\mathbf{r}_i(t) - \mathbf{r}_i(0)|^2 \rangle, \tag{1}$$

$\mathbf{r}_i(t)$ being the position of the ith oxygen atom at a particular time t by use of the relationship
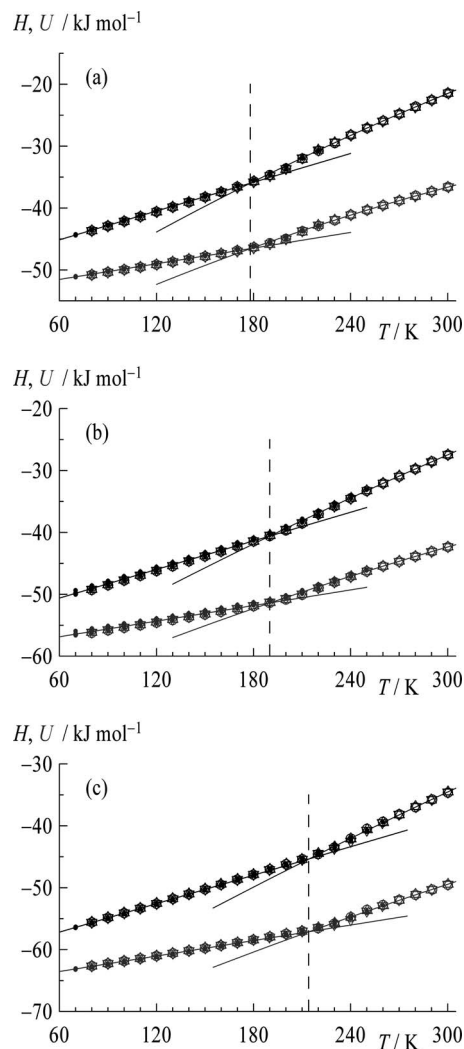

FIG. 4. Total energy (enthalpy) H and potential energy U as a function of temperature T for the (a) COMPASS, (b) TIP3P*, and (c) SPC/E* force fields. Symbols as in Fig. 3. Lines are obtained by linear (left) and polynomial (right) regression of data points belonging to $T < 160$ K and $T > 220$ K, respectively. The intersections reading as (a) 178.0 and 178.2 K, (b) 189.9 and 190.1 K, and (c) 214.5 and 214.2 K represent T_g, indicated by vertical broken lines.

$$D = \frac{1}{6} \lim_{t \to \infty} \frac{d\,msd_t}{dt}. \tag{2}$$

Mean square displacements extracted from *NPT* trajectories using the Andersen thermostat are not suitable to calculate D via Eq. (2) because this thermostat replaces the velocity of molecules in certain intervals afresh from the Maxwell–Boltzmann distribution according to the temperature of the heat bath, thus disturbing the trajectory in a stochastic way. In order to obtain correct diffusion coefficients short *NVE* runs or alternatively *NVT* runs with the Nosé[36] instead of the Andersen thermostat could be performed starting from a representative frame with respect to actual density and pressure. Instead, for all types of ensembles and thermostats, mobility may be assessed directly by mean square displacement, Eq. (1), although the connection to D is lost. Thus, in Fig. 5 msd_{100} values, i.e., mean square displacements achieved after 100 ps, are depicted in a semilogarithmic plot against T. For low temperatures msd_{100} values are
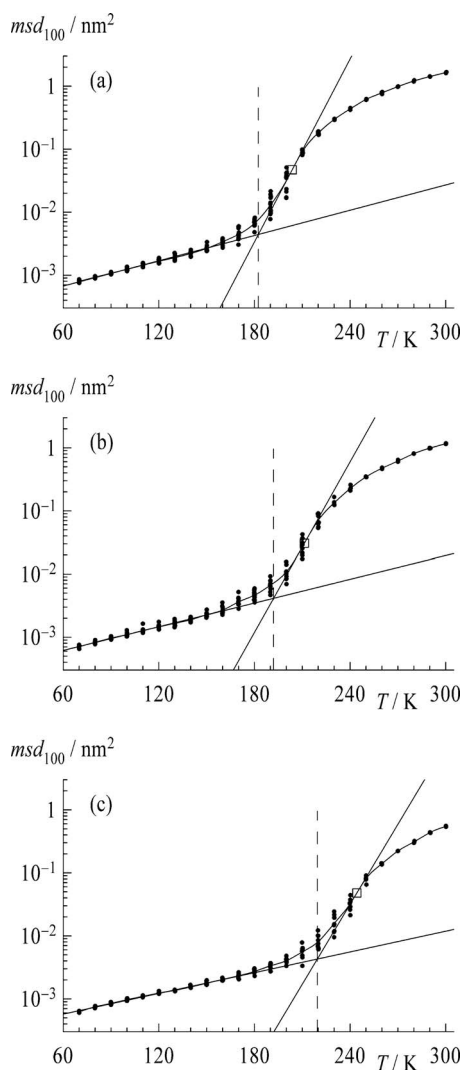
FIG. 5. Mean square displacement of oxygen atoms within 100 ps as a function of temperature T for the (a) COMPASS, (b) TIP3P*, and (c) SPC/E* force fields. Contrary to Figs. 2 and 3 all data are represented by dots. The curves are spline functions through average values at each temperature. The intersection of the limiting slope with the stationary tangent (the point of inflection marked by a square) reading as (a) 182.4, (b) 192.0, and (c) 219.4 K represent T_g, indicated by vertical broken lines.

FIG. 6. Radial density functions between O atoms for the (a) COMPASS, (b) TIP3P*, and (c) SPC/E* force fields for $T = 80$ (black), 120, 160, 200, 240, and 280 K (very light gray), the intensity of the gray scale decreasing with increasing temperature. The figures refer to first coordination numbers $N(0.33)$, see Eq. (3).

rather small and linearly increase on a logarithmic scale. For higher temperatures, however, the msd_{100} values rapidly increase and then level off resulting in S-shaped curves. The onset of the pronounced increase in mobility may be defined as deviation from linear T-dependence which in turn is traced back to the intersection of the limiting tangent at small temperatures and the stationary tangent, reading as ≈ 182, ≈ 192, and ≈ 219 K for COMPASS, TIP3P*, and SPC/E*. These values coincide fairly well with the characteristic temperatures obtained from Figs. 3 and 4 and may be regarded as further independent estimates for the glass transition temperature of high-density water.

E. Radial density profiles

By use of isotope substitution neutron scattering Bowron and co-workers[5,37] studied the structure of various forms of amorphous ice and calculated radial density profiles (pair distribution functions) $g(r)$. A first neighbor coordination
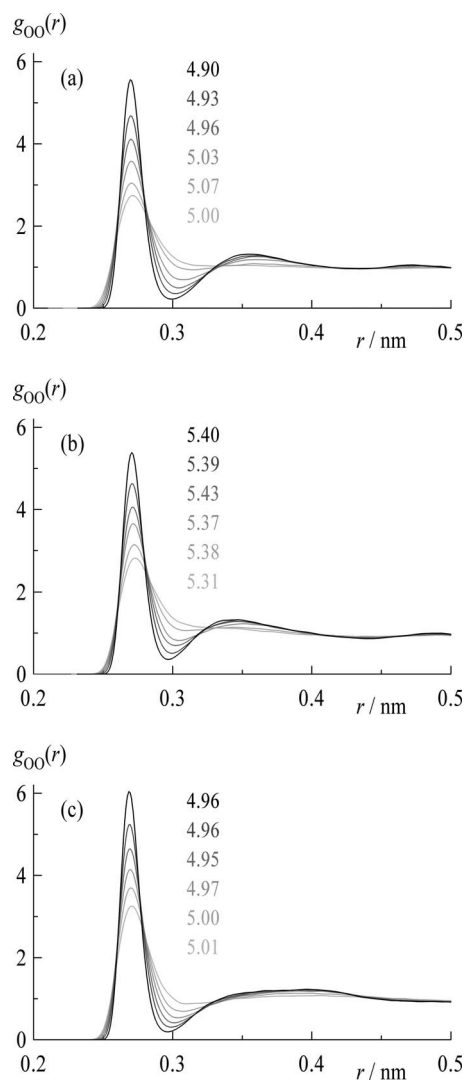
number analysis of the radial density profile of oxygen $g_{OO}(r)$ showed that LDA is almost perfectly fourfold coordinated in the intermolecular distance range from 0.25 to 0.33 nm. HDA and VHDA were found to be fourfold coordinated in the range from 0.25 to 0.31 nm. However, between 0.31 and 0.34 nm the coordination number increases to ≈ 5 for HDA and ≈ 6 for VHDA but remains close to 4 in case of LDA. Analysis of the intermolecular oxygen/hydrogen distribution function $g_{OH}(r)$ revealed a four-coordinated hydrogen bonded network in all cases (two hydrogen bonded hydrogen atoms in a distance of 0.14–0.24 nm from any oxygen atom). These structural differences and similarities should be reflected in the simulated data, too.

In Figs. 6 and 7 $g_{OO}(r)$ and $g_{OH}(r)$ are depicted for six temperatures ranging from 80 to 280 K in steps of 40 K, thus covering the glassy as well as the (ultraviscous) liquid state. As a matter of fact the broadness of the peaks increases with increasing temperature; thus, the curves with the sharpest first peak refer to the lowest temperature and those with the
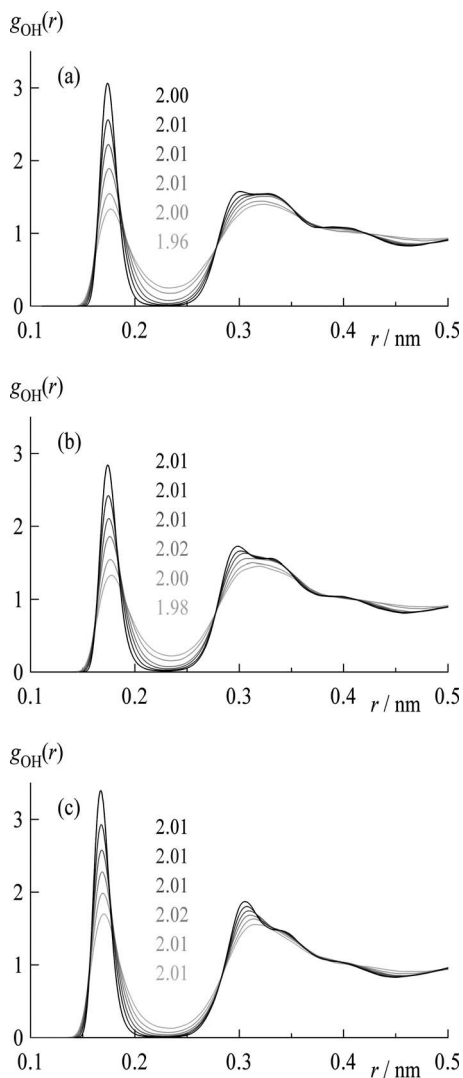
FIG. 7. Intermolecular radial density functions between O atoms and H atoms for the (a) COMPASS, (b) TIP3P*, and (c) SPC/E* force fields for $T=80$ (black), 120, 160, 200, 240, and 280 K (very light gray), the intensity of gray scale decreasing with increasing temperature. The figures refer to first coordination numbers $N(0.24)$, see Eq. (3).

broadest one to the highest. Nevertheless, the principal shape of the curves is retained and the position of the peaks remains nearly unchanged. The first maximum of $g_{OO}(r)$ is located at ≈ 0.27 nm in accordance with the experimental value. The second peak is at $(0.35–0.36)$ nm for COMPASS and TIP3P* and at ≈ 0.4 nm for SPC/E*. Thus, the location of the second peak is at considerably lower radial distances than 0.44 nm reported for LDA giving evidence that the simulations indeed represent HDA ice.

Comparison of Fig. 6 with Fig. 13 of Ref. 5 reveals that the maximum of the second peak of SPC/E* model coincides with the HDA peak while the COMPASS and TIP3P* peak maximum is located between those of VHDA and HDA. The first maximum of $g_{OH}(r)$, see Fig. 7, occurs at ≈ 0.175 nm for COMPASS and TIP3P* and at ≈ 0.170 nm for SPC/E*, the second one at $\approx(0.30–0.32)$ nm, slightly shifting to higher values with increasing temperature, while the minimum lying in between occurs at ≈ 0.23 nm. All these features are in good agreement with the experimental distribution functions given in Fig. 14 of Ref. 5.

Another option to assign the model systems to experimental ice amorphs is given by an analysis of first neighbors. The number of oxygen and hydrogen neighbors, respectively, within a distance r from the center of an O atom may be calculated by

$$N(r) = \int_0^r \rho(r) \cdot 4\pi r^2 dr = \int_0^r g(r) \cdot \bar{\rho} \cdot 4\pi r^2 dr, \qquad (3)$$

with $\rho(r)$ and $\bar{\rho}$ being the distance dependent and average number density of oxygen and hydrogen, respectively, and $g(r)$ either $g_{OO}(r)$ or $g_{OH}(r)$.

The number of nearest (nonbonded) H atoms around O from 0.14 to 0.24 nm, calculated via Eq. (3), is 2.0 for all models in accordance with the experimental result. More interesting is the first neighbor coordination number for oxygen atoms (OO) which significantly differs for LDA, HDA, and VHDA, as stated above. For temperatures up to 200 K, integration over the range of the first peak of $g_{OO}(r)$—the upper limit of integration being the position of the first minimum, $(0.30–0.31)$ nm—yields a coordination number of 4.00 ± 0.05, i.e., perfect fourfold coordination as found experimentally. Integration up to 0.33 nm yields $\approx 5.00 \pm 0.05$ for COMPASS and SPC/E* and a slightly larger value of 5.35 ± 0.05 for TIP3P*. For an upper integration limit of 0.34 nm these values increase to 5.55 ± 0.05 and 6.0 ± 0.1, respectively. Thus, all three models under the simulation conditions chosen represent high-density ices, i.e., COMPASS and SPC/E* obviously HDA while TIP3P* more likely corresponds to VHDA.

IV. CONCLUSIONS

We have employed molecular dynamics simulations to search for the glass-to-liquid transition in HDA ice. At a pressure of $p \approx 0.3$ GPa several heating/cooling cycles for three different model systems (force fields COMPASS, TIP3P*, and SPC/E*) were performed and density, total energy, and molecular mobility (simply defined by the mean square displacement after a certain amount of time) were analyzed as a function of temperature T. In all cases a glass transition temperature T_g is observed, its value depending on the system as well as (slightly) on the method adopted. From the kink in the density profile we estimate T_g to be ≈ 184, ≈ 194, and ≈ 223 K (COMPASS, TIP3P* and SPC/E*), the width of the transition being $\approx 20–30$ K. Slightly smaller values are obtained from the temperature dependence of energies, i.e., ≈ 178, ≈ 190, and ≈ 214 K. T_g values taken from the onset of pronounced increasing mobility are between these values, i.e., ≈ 182, ≈ 192, and ≈ 219 K.

It should be noted that COMPASS based simulations[23] using a smaller system (512 water molecules) in the temperature range [70 K, 220 K] resulted in qualitatively similar profiles, the densities, however, being slightly smaller. In order to check for a systematic dependence of the results on the system size a preliminary run with 2048 water molecules was performed in addition. After relaxation two full temperature cycles yield densities in between those of the systems

containing 512 and 1024 water molecules, respectively. The total energy, as well as the potential energy per mole water, nearly perfectly coincide for all system sizes.

Comparison of radial distribution functions with experimental values determined from neutron diffraction experiments and empirical potential structure refinement[5,37] reveals that the calculations with COMPASS and SPC/E* force fields under the conditions chosen indeed represent HDA, while TIP3P* more likely simulates VHDA.

Even though the temperatures obtained from simulations typically deviate significantly from experimental temperatures, our simulations suggest that HDA (VHDA) ices may indeed be proxies of ultraviscous HDLs (VHDLs) at low temperatures.

ACKNOWLEDGMENTS

[1] C. G. Salzmann, P. G. Radaelli, A. Hallbrucker, E. Mayer, and J. L. Finney, Science **311**, 1758 (2006).

[2] E. F. Burton and W. F. Oliver, Proc. R. Soc. London, Ser. A **153**, 166 (1935); P. Brüggeller and E. Mayer, Nature (London) **288**, 569 (1980); J. Lepault, R. Freeman, and J. Dubochet, J. Microsc. **132**, RP3 (1983); E. Mayer, J. Appl. Phys. **58**, 663 (1985); T. Loerting, C. Salzmann, I. Kohl, E. Mayer, and A. Hallbrucker, Phys. Chem. Chem. Phys. **3**, 5355 (2001); G. Strazzulla, G. A. Baratta, and M. E. Palumbo, Spectrochim. Acta, Part A **57A**, 825 (2001); T. Loerting, W. Schustereder, K. Winkel, C. G. Salzmann, I. Kohl, and E. Mayer, Phys. Rev. Lett. **96**, 025702 (2006).

[3] O. Mishima, L. D. Calvert, and E. Whalley, Nature (London) **310**, 393 (1984).

[4] C. A. Angell, Annu. Rev. Phys. Chem. **55**, 559 (2004).

[5] D. T. Bowron, J. L. Finney, A. Hallbrucker, I. Kohl, T. Loerting, E. Mayer, and A. K. Soper, J. Chem. Phys. **125**, 194502 (2006).

[6] J. Zarzycki, *Glasses and the Vitreous State* (Cambridge University Press, Cambridge, 1991).

[7] C. G. Salzmann, I. Kohl, T. Loerting, E. Mayer, and A. Hallbrucker, Phys. Chem. Chem. Phys. **5**, 3507 (2003); I. Kohl, L. Bachmann, A. Hallbrucker, E. Mayer, and T. Loerting, *ibid.* **7**, 3210 (2005); I. Kohl, L. Bachmann, E. Mayer, A. Hallbrucker, and T. Loerting, Nature (London) **435**, E1 (2005).

[8] G. P. Johari, A. Hallbrucker, and E. Mayer, Nature (London) **330**, 552 (1987); C. A. Angell, J. Phys.: Condens. Matter **19**, 205112 (2007).

[9] O. Andersson, Phys. Rev. Lett. **95**, 205503 (2005); O. Andersson and A. Inaba, Phys. Rev. B **74**, 184201 (2006).

[10] O. Mishima and Y. Suzuki, J. Chem. Phys. **115**, 4199 (2001).

[11] M. Seidl, M. S. Elsaesser, G. Zifferer, E. Mayer, and T. Loerting, "Volumetric Glass-to-Liquid Transition in Amorphous Ices up to 0.3 GPa," Phys. Rev. Lett. (submitted).

[12] J. S. Tse and M. L. Klein, Phys. Rev. Lett. **58**, 1672 (1987); J. Chem. Phys. **96**, 5482 (1992); J. S. Tse, D. D. Klug, C. A. Tulk, I. Swainson, E. C. Svensson, C. K. Loong, V. Shpakov, V. R. Belosludov, R. V. Belosludov, and Y. Kawazoe, Nature (London) **400**, 647 (1999).

[13] O. Mishima, Nature (London) **384**, 546 (1996).

[14] T. Strassle, S. Klotz, G. Hamel, M. M. Koza, and H. Schober, Phys. Rev. Lett. **99**, 175501 (2007).

[15] M. M. Koza, T. Hansen, R. P. May, and H. Schober, J. Non-Cryst. Solids **352**, 4988 (2006).

[16] N. Giovambattista, H. E. Stanley, and F. Sciortino, Phys. Rev. Lett. **94**, 107803 (2005).

[17] R. Martonak, D. Donadio, and M. Parrinello, Phys. Rev. Lett. **92**, 225702 (2004).

[18] I. Brovchenko, A. Geiger, and A. Oleinikova, J. Chem. Phys. **118**, 9473 (2003).

[19] T. Loerting and N. Giovambattista, J. Phys.: Condens. Matter **18**, R919 (2006); I. Brovchenko and A. Oleinikova, J. Chem. Phys. **124**, 164505 (2006); R. V. Belosludov, O. S. Subbotin, H. Mizuseki, P. M. Rodger, Y. Kawazoe, and V. R. Belosludov, *ibid.* **129**, 114507 (2008).

[20] P. H. Poole, U. Essmann, F. Sciortino, and H. E. Stanley, Phys. Rev. E **48**, 4605 (1993); C. J. Roberts, P. G. Debenedetti, and F. H. Stillinger, J. Phys. Chem. B **103**, 10258 (1999); I. Brovchenko, A. Geiger, and A. Oleinikova, J. Chem. Phys. **123**, 044515 (2005); R. Martonak, D. Donadio, and M. Parrinello, *ibid.* **122**, 134501 (2005); N. Giovambattista, H. E. Stanley, and F. Sciortino, Phys. Rev. E **72**, 031510 (2005); J. Slovak and H. Tanaka, J. Chem. Phys. **122**, 204512 (2005); C. Vega, C. McBride, E. Sanz, and J. L. F. Abascal, Phys. Chem. Chem. Phys. **7**, 1450 (2005); D. Paschek, Phys. Rev. Lett. **94**, 217802 (2005).

[21] M. S. Elsaesser, I. Kohl, E. Mayer, and T. Loerting, J. Phys. Chem. B **111**, 8038 (2007).

[22] N. Giovambattista, C. A. Angell, F. Sciortino, and H. E. Stanley, Phys. Rev. Lett. **93**, 047801 (2004); J. Liu, S.-Y. Wang, C.-P. Zheng, L.-J. Xin, D. Wang, and M.-H. Sun, Chin. Phys. Lett. **24**, 2025 (2007).

[23] M. Seidl, T. Loerting, and G. Zifferer, "Molecular Dynamics Simulations on the Glass-to-Liquid Transition in High Density Amorphous Ice," Z. Phys. Chem. (in press).

[24] T. A. Andrea, W. C. Swope, and H. C. Andersen, J. Chem. Phys. **79**, 4576 (1983).

[25] H. C. Andersen, J. Chem. Phys. **72**, 2384 (1980).

[26] L. Verlet, Phys. Rev. **159**, 98 (1967).

[27] M. J. Hwang, T. P. Stockfisch, and A. T. Hagler, J. Am. Chem. Soc. **116**, 2515 (1994); H. Sun, Macromolecules **28**, 701 (1995); H. Sun, J. Phys. Chem. B **102**, 7338 (1998); H. Sun, P. Ren, and J. R. Fried, Comput. Theor. Polym. Sci. **8**, 229 (1998);; S. W. Bunte and H. Sun, J. Phys. Chem. B **104**, 2477 (2000).

[28] D. Rigby, Fluid Phase Equilib. **217**, 77 (2004).

[29] W. L. Jorgensen, J. Chandrasekhar, J. D. Madura, R. W. Impey, and M. L. Klein, J. Chem. Phys. **79**, 926 (1983).

[30] H. J. C. Berendsen, J. R. Grigera, and T. P. Straatsma, J. Phys. Chem. **91**, 6269 (1987).

[31] P. Dauber-Osguthorpe, V. A. Roberts, D. J. Osguthorpe, J. Wolff, M. Genest, and A. T. Hagler, Proteins **4**, 31 (1988).

[32] K. G. Wagner, M. Maus, A. Kornherr, and G. Zifferer, Chem. Phys. Lett. **406**, 90 (2005); M. Maus, K. G. Wagner, A. Kornherr, and G. Zifferer, Mol. Simul. **34**, 1197 (2008).

[33] A. Simperler, A. Kornherr, R. Chopra, P. A. Bonnet, W. Jones, W. D. S. Motherwell, and G. Zifferer, J. Phys. Chem. B **110**, 19678 (2006).

[34] M. P. Allen and D. J. Tildesley, *Computer Simulation of Liquids* (Oxford Science Publications, Oxford, 1987).

[35] A. Simperler, A. Kornherr, R. Chopra, W. Jones, W. D. S. Motherwell, and G. Zifferer, Carbohydr. Res. **342**, 1470 (2007).

[36] S. Nose, Mol. Phys. **52**, 255 (1984).

[37] J. L. Finney, A. Hallbrucker, I. Kohl, A. K. Soper, and D. T. Bowron, Phys. Rev. Lett. **88**, 225503 (2002).